# Atmospheric Correction Algorithms Assessment for Sentinel-2A Imagery over Inland Waters of China

## Case Study, Qiandao Lake

Allam, Mona; Meng, Qingyan; Elhag, Mohamed; Giardino, Claudia; Ghirardi, Nicola; Su, Yi; Al-Hababi, Mohammed A.M.; Menenti, Massimo

**DOI**
10.1007/s41748-023-00366-w

**Publication date**
2024

**Document Version**
Final published version

**Published in**
Earth Systems and Environment

**Citation (APA)**
Allam, M., Meng, Q., Elhag, M., Giardino, C., Ghirardi, N., Su, Y., Al-Hababi, M. A. M., & Menenti, M. (2024). Atmospheric Correction Algorithms Assessment for Sentinel-2A Imagery over Inland Waters of China: Case Study, Qiandao Lake. *Earth Systems and Environment*, *8*(1), 105-119. https://doi.org/10.1007/s41748-023-00366-w

Earth Systems and Environment
https://doi.org/10.1007/s41748-023-00366-w

ORIGINAL ARTICLE

# Atmospheric Correction Algorithms Assessment for Sentinel-2A Imagery over Inland Waters of China: Case Study, Qiandao Lake

**Mona Allam[1,4] · Qingyan Meng[1,2,3] · Mohamed Elhag[5,6,7,8] · Claudia Giardino[9] · Nicola Ghirardi[9] · Yi Su[10] · Mohammed A. M. Al-Hababi[11] · Massimo Menenti[12]**

Received: 26 June 2023 / Revised: 8 December 2023 / Accepted: 12 December 2023


**Abstract**
Around 90% of the oceanic and inland waters' reflectance registered in satellite detectors comes from the atmospheric contribution. Hence the water-leaving radiances in the Near-InfraRed (NIR) region are above the zero value over inland waters because of sediments and dissolved organic particles, this radiance cannot be ignored. To accurately retrieve water quality parameters from water-leaving reflectance, atmospheric correction is the most important step. This study evaluated five reliable atmospheric correction algorithms (AC) known as: (ACOLITE, C2RCC, iCOR, 6SV, and Sen2Cor) against optical in-situ measurements collected above the water in Qiandao Lake, China using Sentinel-2 Multi-Spectral Imager. 60 in-situ water samples and optical measurements (range 400–900 nm) above the water were collected at different points in Qiandao Lake. The spectra measurements were used to validate the atmospheric correction processors. All ACs that were evaluated showed high levels of uncertainty. ACOLITE and ICOR performed the best statistics with root mean square differences (RMSD) (0.006 $sr^{-1}$) while Sen2Cor achieved the lowest RMSD (0.023 $sr^{-1}$) across the different modules. ACOLITE, had a better performance when applied to meso- and hypereutrophic waters, compared with oligotrophic, while C2RCC performs better at the wavelength of 833 nm (0.007 $sr^{-1}$). Finally, 6S performs better at the wavelength of 665 nm (0.015 $sr^{-1}$). This study introduces insights and addresses a significant research gap in the field of atmospheric correction for satellite imagery over inland waters. Prior studies have primarily focused on atmospheric correction algorithms for coastal and open ocean environments while few studies focused on the unique characteristics and challenges associated with inland water bodies. The findings of this study are crucial for researchers, remote sensing experts, and environmental scientists working with Sentinel-2A imagery, as it enables them to make more accurate and reliable interpretations of water quality and other environmental parameters derived from satellite data.

**Keywords** Atmospheric correction · Sentinel-2 · Qiandao Lake · Inland Water

## 1 Introduction

### 1.1 Water Quality Problem in Lake Qiandao

The Qiandao Lake, also called the Xin'anjiang Reservoir, is situated in the western portion of the Chinese province of Zhejiang. It is the largest (580 $km^2$) and deepest reservoir (about 34 m on average) in China, and represents a significant water source (Li et al. 2021a; Wu et al. 2015) and is developed sustainably in eastern China (Gu et al. 2016a). Hence, monitoring the water environment of Qiandao Lake is a crucial aspect of reservoir management. Unfortunately, due to rapid growth in the surrounding area, fertilizer and other contaminants have increasingly invaded the lake (Zeng et al. 2020; Wang et al. 2018). Simis et al. (2005) reported that according to the results of monthly field measurements carried out at five different locations in the lake between 2002 and 2011, the mean chlorophyll values were between 2.72 and 1.38 $mg/m^3$ annually. The results that were collected from the satellite showed that the surface chlorophyll annual mean value was less than 3.65 $mg/m^3$ (Gu et al. 2016b).

Generally, Qiandao Lake exhibited oligotrophic conditions (Carlson 1977). In this regard, Yang et al. (2013) measured the trophic state index between 2007 and 2011, observing an annual mean value of 26.6 Furthermore, several modeling, and field studies have helped to increase our understanding of changes in the ecosystem of the entire area

Extended author information available on the last page of the article

Published online: 18 January 2024

of the lake and its surroundings. Blooms and eutrophication were detected in Qiandao Lake during the 1990s. These changes can be largely ascribed to an increase in input nutrients, generated by human activity (Wu et al. 2015). Although Qiandao Lake has many environmental problems, the water quality spatiotemporal distribution in the lake of and how they affect the environment is still unclear. Thus, it is important to observe the water quality of this lake. Remote sensing approaches are reliable and powerful tools that can estimate the near-surface Chl-*a* concentrations of the inland waters (Zeng et al. 2020).

### 1.2 Remote Sensing and Water Quality Studies

The European Space Agency (ESA) launched the Sentinel-2A instrument as a series of Multi-Spectral Imager (MSI) nearly in June 2015. This satellite is characterized by a revisit time of 10 days, but which is reduced to 5 days with the introduction of Sentinel-2B. These satellites are characterized by a spatial resolution of 10–60 m depending on the band. The instrument was designed principally as a terrestrial-monitoring component of the Copernicus program. Nevertheless, MSI kept recording coastal marine areas that can be useful for other monitoring purposes including the inshore water quality areas and inland water bodies that are not detectable by Ocean Colour Sensors like OLCI (Sentinel-3). The design of the MSI optical waveband is comparable to that of former terrestrial-monitoring satellites such as NASA/USGS Landsat 7 and 8. These instruments have proven consistent in water remote sensing applications (Bresciani et al. 2018; Pahlevan et al. 2017a; Vanhellemont and Ruddick 2015; Khattab and Merkel 2014; Dona et al. 2015). The 705 nm band of the MSI was designed to map the essential "red edge" behavior which is an essential wavelength to detect accurately the Chlorophyll as well as the inland water bodies (Bresciani et al. 2018).

### 1.3 Atmospheric Correction as an Important Step in Monitoring Water Quality

The optically active components (OACs) that interact with sunlight include phytoplankton, Colored Dissolved Organic Matter (CDOM), non-algal particles (NAP), and suspended sediment. These OACs have a significant contribution to the water radiance that satellite instruments measure. Moreover, the atmosphere, composed by gases and aerosols, also contributes to the water radiance (Warren et al. 2019). The atmospheric path-radiance in the visible portion of the spectrum is at least 80–90% higher than water-leaving radiance (Warren et al. 2019; Gordon et al. 1985; Gordon 1978; Harmel et al. 2018). This is mostly due to the scattering in the atmosphere due to aerosol molecules' presence decreases with the wavelength increases. These signal components need to be removed in order to measure the actual reflection of the water surface. Whitecaps (Wang and Bailey 2001; Steinmetz et al. 2011; Gordon 1997; Gordon and Wang 1994; Richter 1990) as adjacency (Reinersman and Carder 1995; Santer and Schmechtig 2000; Keukelaere et al. 2018; Moses et al. 2017) can also be considered as additional influences. These effects produce an additional signal and can complicate their removal (Mograne et al. 2019). Therefore, any AC method basically subtracts the atmospheric contribution in terms of sunglint, aerosols scattering, and/or whitecaps from the TOA signal (Richter 1990). As a result, there is a need to assess the effectiveness of various AC algorithms in order to better retrieve inland water quality. The inland water bodies represent our main supplies of potable water, are often for recreational uses, and have a high level of biodiversity (40%( of freshwater and marine biomass) (Groetsch et al. 2017). The in-situ data were collected from handheld and shipborne spectrometers may possibly be viewed as atmospheric effects-free due to the optical path from the sensor to the observed target being mainly negligible (Gordon et al. 1985). These observations can, therefore, be used as a source of validation for the AC (Simis and Olsson 2013; Doxani et al. 2018). AC's processors and reflectance products have previously been evaluated in previous studies (Warren et al. 2019; Gordon et al. 1985; Gordon 1978, 1997; Harmel et al. 2018; Wang and Bailey 2001; Steinmetz et al. 2011; Gordon and Wang 1994; Richter 1990; Reinersman and Carder 1995; Santer and Schmechtig 2000; Keukelaere et al. 2018; Moses et al. , 2017; Mograne et al. 2019; Groetsch et al. 2017; Simis and Olsson 2013; Doxani et al. 2018; Xu et al. 2020). For example, ACIX has evaluated the performance of ACOLITE and SeaDAS (Warren et al. 2019). Moreover, Gordon et al. (1985) compared above-water optical in-situ observations to six publicly accessible atmospheric correction algorithms (ACOLITE, C2RCC, iCOR, l2gen, Polymer, and Sen2Cor) and discovered that Polymer and C2RCC achieved the lowest Root Mean Square Difference (RMSD). This study also revealed that further developments AC algorithms are needed to map accurately the spectral shape in the Red and NIR domains in order to retrieve chlorophyll-a concentrations with precision. The main objective of this work is to evaluate five selected AC algorithms, applied to Sentinel-2 data: ACOLITE, Case 2 Regional Coast Color (here referred to as C2RCC), Image correction for atmospheric effects (iCOR), Sentinel-2 Correction (Sen2Cor), and Second Simulation of a Satellite Signal in the Solar Spectrum (6SV). All of these processors are available free of charge to users, and the results produced by each processor will be validated using in-situ measurements of water properties.

The research article makes significant contributions to our understanding of the conceptual basic correction algorithms for Sentinel-2A satellite imagery over inland waters.

By assessing various algorithms, the study provides valuable insights into their performance and identifies the most effective approaches for accurate atmospheric correction in these specific environments. This research enhances our understanding by shedding light on the challenges and limitations associated with atmospheric correction over inland waters and proposing solutions to overcome them. The novelty lies in the comprehensive assessment of these algorithms, considering factors such as, adjacency effects, and specific atmospheric conditions prevalent in inland water regions. By doing so, this research article contributes to the development of more accurate and reliable atmospheric correction techniques for Sentinel-2A imagery over inland waters, thus enabling improved monitoring and understanding of these crucial ecosystems.

## 2 Materials and Methods

### 2.1 Study Area

Qiandao Lake lies between latitudes 29° 11′ and 30° 15′ N and longitudes 118° 34′ and 119° 15′ E (Fig. 1). It is a man-made water body built for the construction purposes of Xin'anjiang Hydropower Station. This region is characterized by a distinctively subtropical monsoon climate, with an average annual temperature of 17.8 °C. It has a capacity of 17.8 billion $m^3$, a width of 150 km, a maximum depth of 30 m, an annual average precipitation of 1489 mm, and an average water retention time of two years. The Xin'anjiang River, Wuqiangxi River, and Fuqiangxi River, respectively, contribute 60%, 20%, and 10%, respectively, of the mean incoming inflow to the Xin'anjia Reservoir annually (Zeng et al. 2020).

### 2.2 In Situ Observation Data

Nanjing Normal University campaigns (Li et al. 2021a) collected data on Lake Qiandao above-water reflectance and water properties in May 2020. As a result, 60 water samples were collected, and radiometric measurements were carried out concurrently at each sampling site (Fig. 1). The study area includes trophic levels ranging from ultraoligotrophic to eutrophic along a broad gradient (Table 1). Applying the classification system for trophic levels suggested by the Organization for Economic Co-operation and Development for lake waters (Warren et al. 2019), of the 60 collected samples, 22 belong to water Type 1 and 38 to water Type 2.

Spectroradiometer device was used to measure the near water surface reflectance Rrs($\lambda$). In the studies by Zeng et al. (2020) and Brockmann et al. 2016), all information regarding the measurement of Rrs($\lambda$) was provided. At, respectively, sampling site, the total water-leaving radiance $L_t$, the sky-viewing radiance $L_{sky}$, and the radiance reflected by a

**Table 1** Classification scheme by water type in Qiandao Lake (Li et al. 2021)

| Water type | Description | Chl-*a* (mg $m^{-3}$) |
|---|---|---|
| Type 1 | Ultraoligotrophic to oligotrophic | < 2.5 |
| Type 2 | Mesotrophic-to-eutrophic | 2.5–25 |
| Type 3 | Hypertrophic | > 25 |

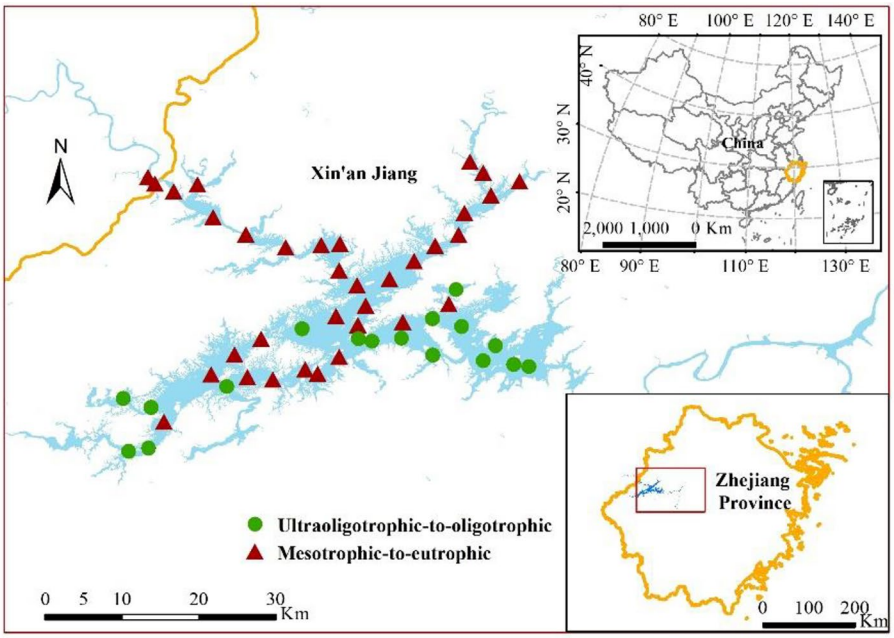


**Fig. 1** Locations of sampling points in Qiandao Lake, May 2019. Green dots mean samples which Chl-*a* < 2.5, red dots means samples which 2.5 < Chl-*a* < 25

standard gray panel $L_p$ were registered. The computation of Rrs($\lambda$) is as follows:

$$\mathrm{Rrs}(\lambda) = \frac{\rho_p\left(L_t - r_{aw}L_{sky}\right)}{\left(\pi L_p\right)} \quad (1)$$

where $\rho_p$ is the reflectance of the gray panel and $r_{aw}$ is the skylight reflectance at the air–water surface (in our case 2.2%). The in-situ collected spectra used in the current study covers wide spectral ranges, including the MSI spectral bands (Fig. 2).

## 2.3 Earth Observation Data and Atmospheric Correction

Sentinel-2 was developed specifically for use in land research purposes, but because to its spatial resolution (10–60 m), advance radiometric resolution, appropriate band configuration, and a short temporal resolution, it may also be used for inland water studies. This makes Sentinel-2 an appropriate remote monitoring for lakes, reservoirs, and coastal waters. In this study, one S2-MSI L1 synchronous scene was downloaded from the Copernicus Open Access Hub of the European Space Agency (https://scihub.copernicus.eu) to match up the field campaign day, 24 May 2020. The image was resampled to a spatial resolution of 10 m using SNAP-ESA Sentinel Application Platformv2.0.2, before applying ACs. The spatial resolution merging across all bands is chosen to enhance the signal/noise ratio and also ease the application of AC. Then, sampled TOA reflectance data atmospherically corrected. In this study, five atmospheric corrections (AC) processors are evaluated: C2RCC v1.0 (Drusch et al. 2012; Main-Knorn et al. 2017), Sen2Cor v2.4.0 (Vermote et al. 1997), ACOLITE 20221025., iCOR v1.0 (Moses et al. 2017), and the Second Simulation of a Satellite Signal in the Solar Spectrum—Vector (6SV) (Sterckx et al. 2015). Figure 3 shows the methodology of the study.

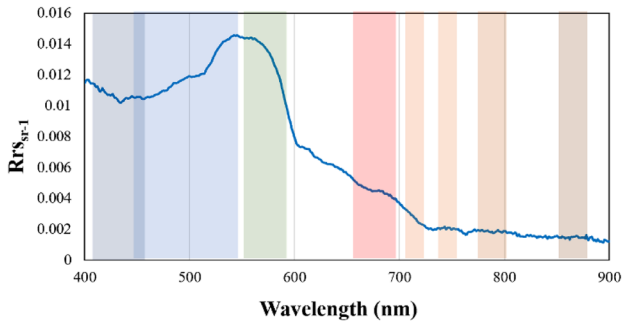


**Fig. 2** In-situ mean spectra demonstrating a characteristic reflectance for each region. Vertical bars illustrates the Sentinel-2B MSI bands corresponding

C2RCC algorithm is a multi-sensor per-pixel artificial neural network (ANN) process in which the ANNs were trained using a huge database of simulated water-leaving and related TOA radiances. The trained ANN datasets were used to convert TOA radiances to water-leaving radiance. In addition, it can generate Chl-*a* maps and calculate water body IOPs. C2RCC processor requires air pressure, temperature, ozone, and salinity as input parameters in addition to calibrated TOA reflectances. The enduring parameters were processed using the processing default parameters (Gordon et al. 1985).

iCOR, formally referred to as OPERA (Guanter et al. 2007), is an approach to correct the atmosphere of land and aquatic targets. First, terrestrial and aquatic pixels are identified, and then Land pixels are utilized to calculate Aerosol Optical Thickness (AOT) based on Berk et al. (2006). Using SIMEC (Guanter et al. 2007), the adjacency correction is performed over water. iCOR employs MODTRAN 5 (Pereira-Sandoval et al. 2019) Look Up Tables (LUT) to

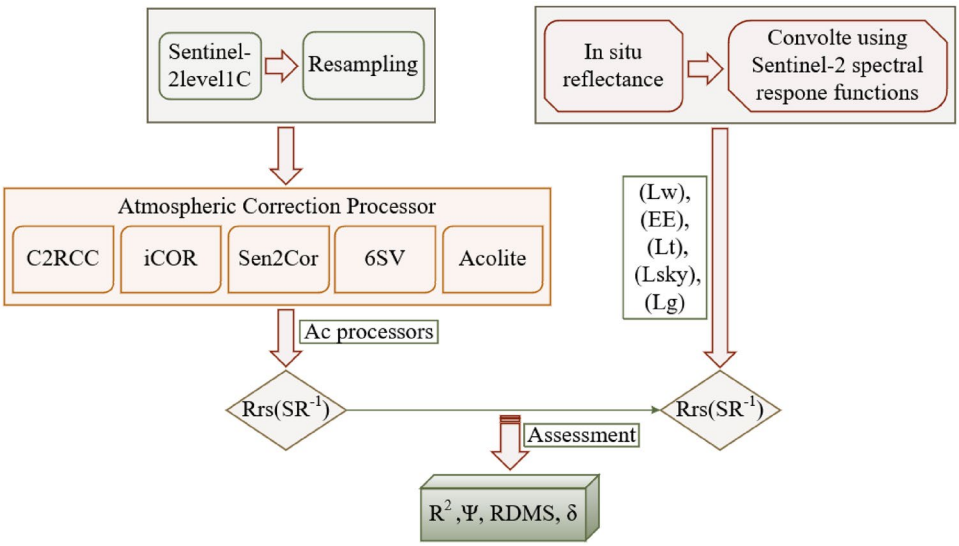


**Fig. 3** Converting top of atmosphere reflectance (TOA) to remote sensing reflectance (Rrs)

implement the atmospheric correction. iCOR requires Solar and Sensor viewing angles, (as well as a digital elevation model (DEM) (Kaufman and Sendra 1988). In this study, the image was processed using the default processing parameters, with the SIMEC adjacency correction applied.

Sentinel-2 Correction (Sen2Cor) is Dense Dark Vegetation (DDV)-based module (Gao et al. 2009; Vanhellemont 2019). This latter implies the vegetation is entirely dark and the atmosphere's reflectance bottom ratios are constant at all wavelengths, necessitating that some pixels in the image correspond to DDV. Once dark pixels exist, the algorithm automatically selects them and corrects the image (Vanhellemont 2019). It is considered a Lambertian surface, while the air and/or water interfaces have a specular reflection (Vanhellemont and Ruddick 2018). The default settings were used to process Sentinel-2 images.

The Management Unit of the Mathematical Model of the North Sea (MUMM) in Belgium developed the AC algorithm ACOLITE for coastal and inland seas (Vanhellemont and Ruddick 2018). The latter uses the dark spectrum fitting approach in principle; nonetheless, it can be adjusted to implement the exponential extrapolation method (Kotchenova et al. 2006). ACOLITE combines diverse aerosol correction techniques for Sentinel-2 data applications including Turbid water. After Rayleigh correction, two bands of aerosol reflectance are produced from the images based on the method selected in the settings.

6SV is a Radiative Transfer (RT) code designed to calculate the look-up tables in terms of AC algorithms for the Moderate-resolution Imaging Spectroradiometer (MODIS) sensor (Sterckx et al. 2015; Liu et al. 2015; Park and Ruddick 2005). It is one of the most used, rigorously validated, in addition to well-known RT published codes within the field of scientific remote sensing. In the current study, the atmospheric profile was defined as "Mid-latitude Summer" according to the geo-location and time of sampling. The aerosol optical depth at 550 nm ($AOD_{550}$) was acquired from MODIS Deep Blue (DB) AOD product retrieved at the same day of sampling. Continental aerosol model was selected as the aerosol type for 6SV model, according to previous study (Pahlevan, et al. 2017b). Two of the processors (C2RCC and ACOLITE) are specifically designed for water bodies, whereas iCOR was developed for use on land and in inland waters, it is not appropriate for use in open water. Sen2Cor is not intended for use in water. However, it is considered in current research because it is the default L2A AC algorithm. Each of the AC methods considers the screening and the illumination of solar angles, and in certain instances, a water model as well (Mobley 1999), or radiative transfer model. The default parameters for each processor were used, along with suggested alternatives for water correction. Those parameters considered to be the optimum configurations for general use deprived of acquaintance of the water bodies or atmospheric conditions. The specific settings, and the data used were defined in Table 2 (Gordon et al. 1985).

## 2.4 In Situ Data Processing

The Spectral Response Functions of Sentinel-2 sensor (S2–SRF) v3.0 were applied to convolute the in-situ spectral reflectance (Vanhellemont and Ruddick 2018). The results were estimated using the approach provided by Main-Knorn et al. (2017). Five measurements, including total water-leaving radiance ($L_w$) and total downward irradiance ($E_E$), total observed radiance ($L_t$), the radiance of the sky ($L_{sky}$), and contribution diffuse sunlight reflected by the water surface ($L_g$) were collected at each water sampling point. The following equations were used to estimate the in-situ reflectance (Rrs):

$$\mathrm{Rrs}(\lambda) = \frac{L_w}{E_E} \tag{2}$$

$$L_w = L_t - L_g \tag{3}$$

$$L_g = \mathrm{rho} \times L_{sky} \tag{4}$$

## 2.5 Extraction of Reflectances

For the S2-MSI images, the reflectances were extracted from a $3 \times 3$ ROI (Region of interest, equivalent to $30 \times 30$ m). Then, the mean in-situ spectral signature was calculated. Using a series of statistical parameters, a comparison was made between the in-situ reflectance and those collected by S2-MSI. This involved the determination coefficient ($R^2$), the Mean Absolute Percentage Difference ($\Psi$), the Root Mean Square Difference (RMSD), and the Mean Relative

**Table 2** AC processors and options selected

| | ACOLITE | C2RCC | iCOR | Sen2COR | 6S |
|---|---|---|---|---|---|
| Input data | TOA reflectances | TOA reflectances | TOA reflectances | TOA reflectances | TOA radiances |
| Output resolution | 10 m | 10 m | 10, 20, 60 m | 10, 20, 60 m | 10 m |
| Other information | SWIR-NIR estimation | 0.001 for salinity, 108 m for elevation | SIMEC adjacency correction (Guanter et al. 2007) | | Automatic aerosol type, mild-latitude and ozone |

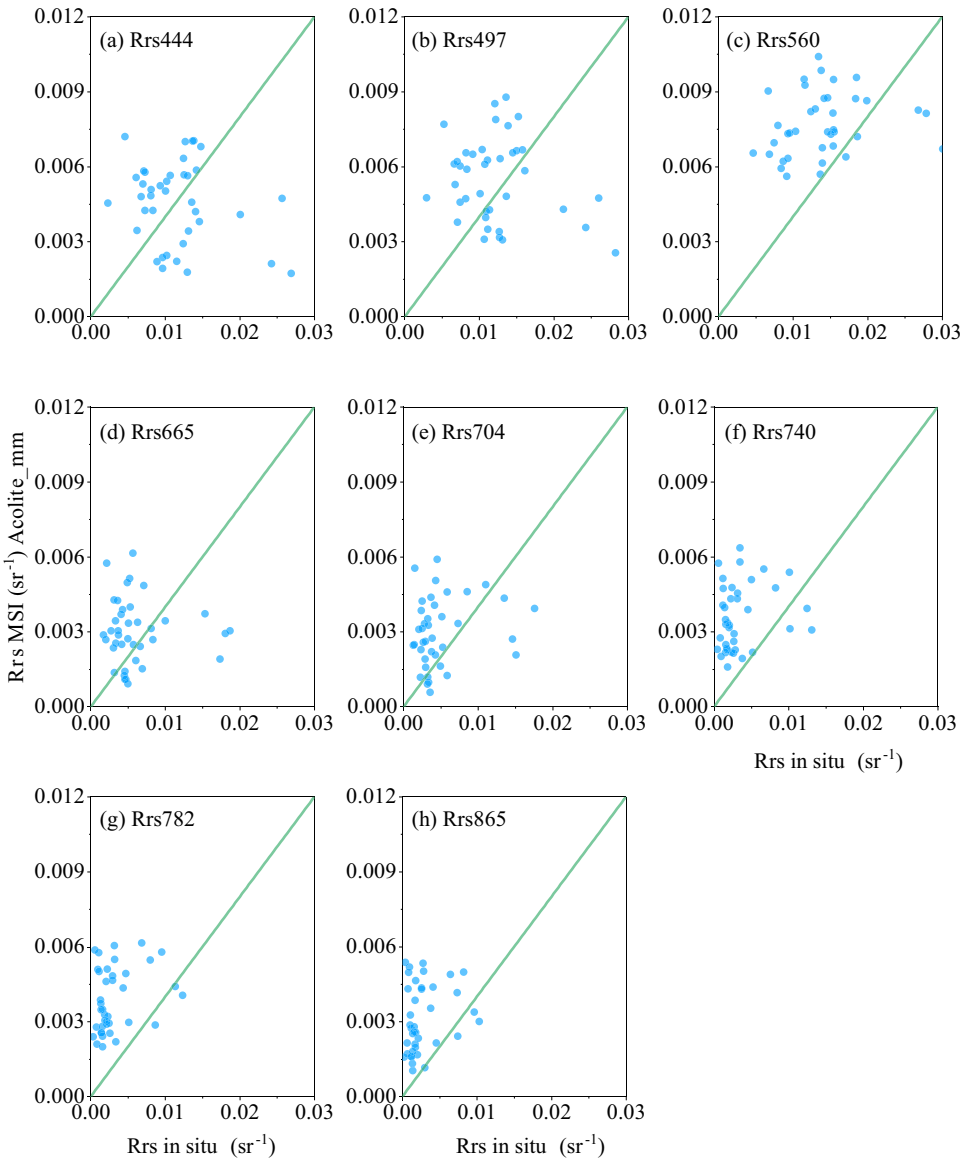


**Fig. 4** ACOLITE per-band scatterplot

Difference ($\delta$). Those metrics were described, respectively, as follows:

$$R^2 = \frac{(\sum(x_i - \bar{x})(y_i - \bar{y}))^2}{\sum(x_i - \bar{x})^2 \sum(y_i - \bar{y})^2} \tag{5}$$

$$\psi = \frac{100}{N}\left|\frac{x_i - y_i}{y_i}\right| \tag{6}$$

$$\text{RMSD} = \sqrt{\frac{1}{N}\sum(x_i - y_i)^2} \tag{7}$$

$$\delta = \frac{1}{N}\sum\frac{(x_i - y_i)}{y_i} \tag{8}$$

## 3 Result

### 3.1 Summary of Pre-processing Analyses

Banding between the detectors can be seen in the data as a result of the different air path lengths. This is because MSI is composed of data from multiple detectors. As the results of different wave lengths for the bands, in addition to MSI is composed from data from multiple detectors, banding was present in all bands after atmospheric corrections.

### 3.2 Qiandao Lake Match-Up Analysis

The scatter plots comparing the on-site spectra to each AC processor's spectral performance are shown in Figs. 4, 5, 6, 7 and 8. Figure 9, on the other hand, shows all the results

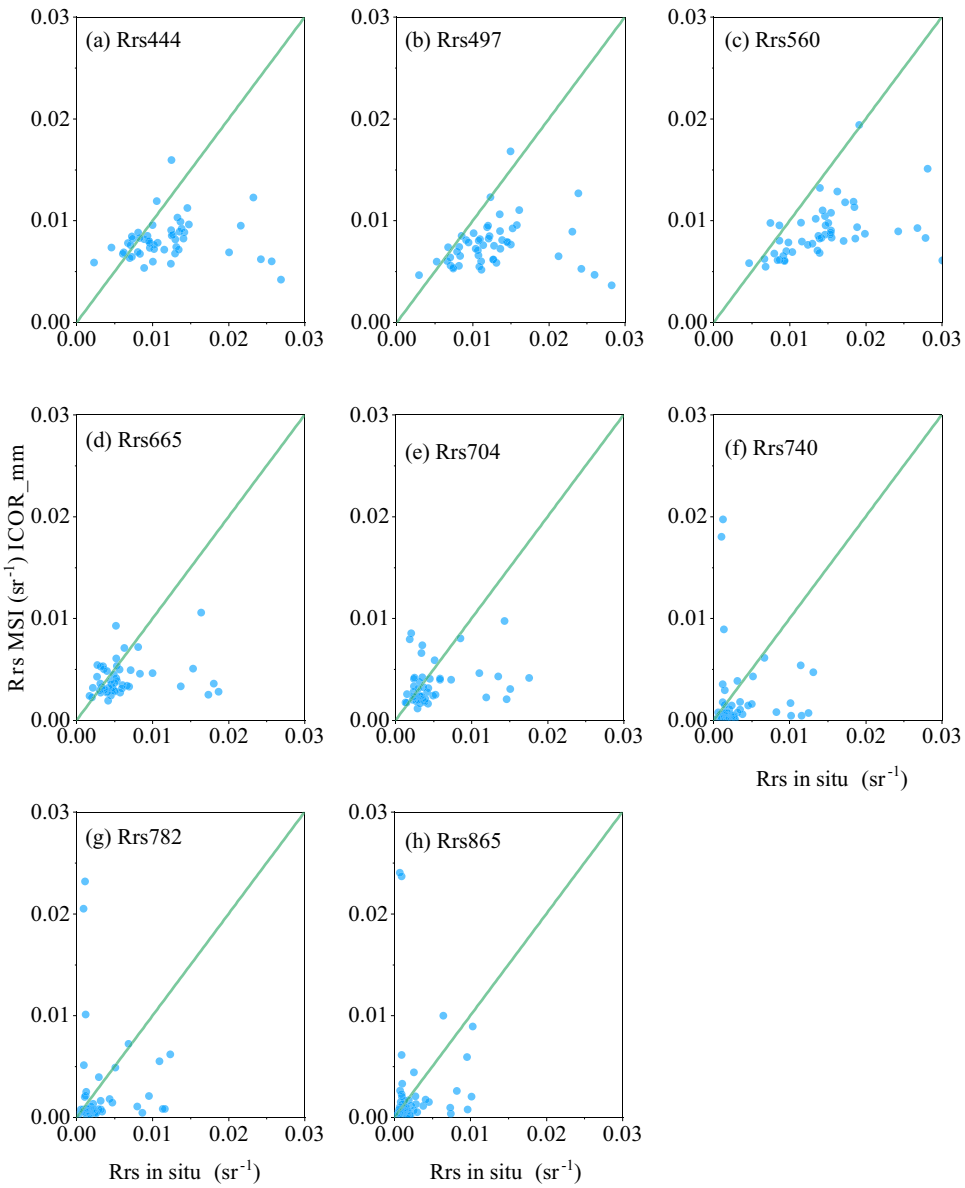


**Fig. 5** iCOR per-band scatterplot

of the statistical indices for the 5 ACs. The algorithms performed similarly in the Qiandao Lake. In general, ACOLITE, iCOR and C2RCC showed the best performance, though with clear biases with RMSD from 0.006 (ACOLITE and iCOR) to 0.007 (C2RCC). 6SV and Sen2COR show lower mean RMSD from 0.016 (6SV) to 0.023 (Sen2COR). 6SVcorrection ranked third at shorter wavelengths ($\leq$600 nm) from the perspective of R.

### 3.3 Combined and Common Match-Up Dataset

In-situ reflectances were compared with measured reflectances generated from S2 images. These comparisons were used to generate descriptive statistics to evaluate the performance of the algorithms used. The statistical findings for each dataset are displayed in Appendix 1. ACOLITE and iCOR showed the best results, producing the lowest RMSD, while iCOR tended to give the higher R2. For 6SVhigh, RMSD for eight wavelengths was observed.

## 4 Discussion

The radiation that reaches the satellite sensor interacts with the aquatic and atmospheric systems in various ways. 70–90% of the signals measured by the sensors come from the atmosphere. This noise must be eliminated to acquire the water-leaving reflectance, the actual signal coming from the water surface. The light detected by the sensor is also

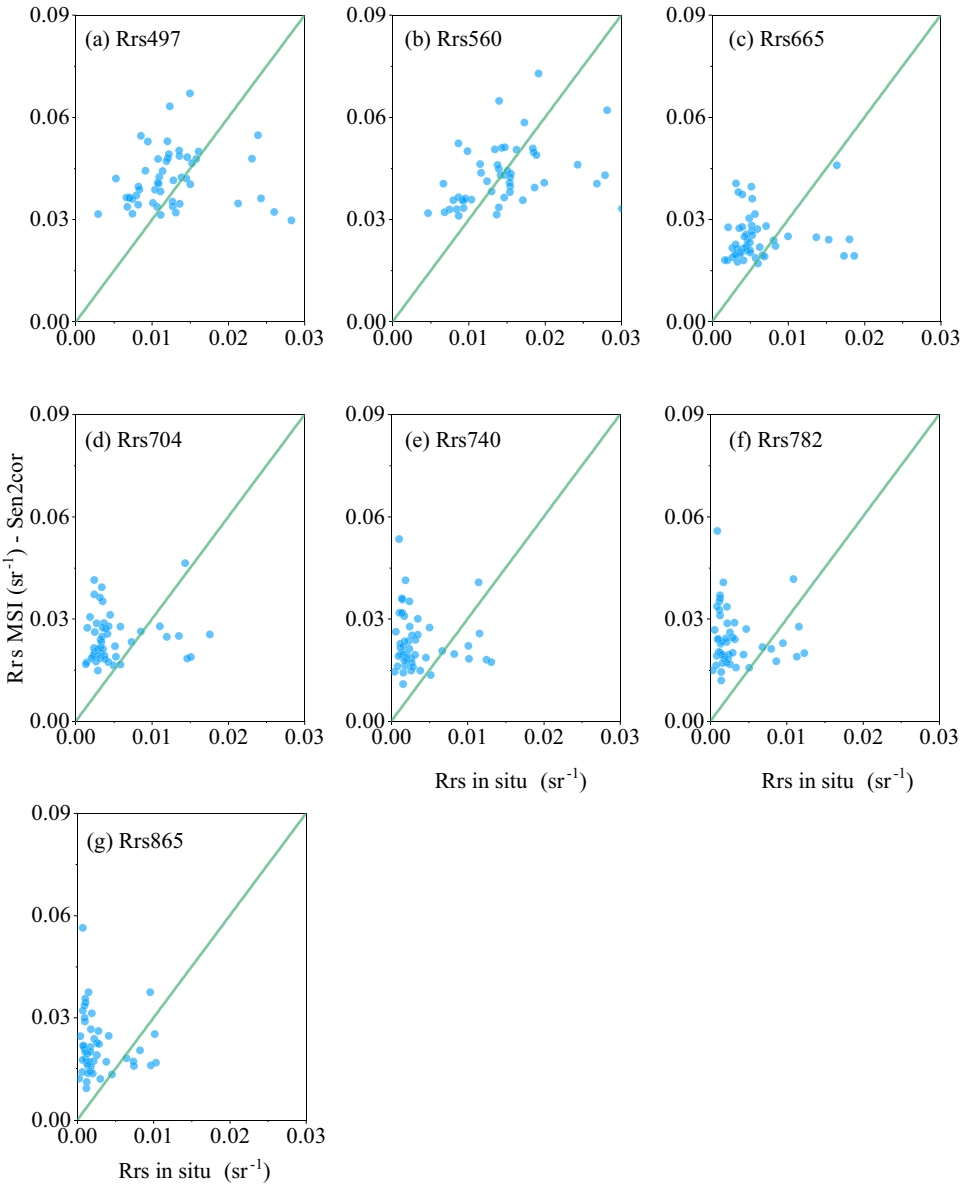


**Fig. 6** Sen2COR per-band scatterplot

affected by outside elements such as sunglint, wind speed, observation geometry, solar angles, and possible land adjacency effects. This led to the development of several AC algorithms concentrating on coastal, oceanic, and inland waters (Pyo et al. 2022). Due to these issues, validation of the reflectance derived from AC processors is required. In this study, five atmospheric corrections processors applied to S2-MSI is tested, analyzed, and validated against in-situ reflectance over Qiandao Lake. In general, two distinct groupings can be distinguished: ACOLITE, iCOR and C2RCC, that replicated the spectral structure of the in-situ data most accurately, and Sen2COR and 6S that show less favorable results. To evaluate the spectral dependence errors for each processor, a statistical analysis was conducted on all bands of the S2. The statistics for each AC algorithm estimated for Qiandao Lake are shown in Table 3. ACOLITE and iCOR performed best and achieved the lowest RMSD (0.006). This suggests that they best reproduced the spectral shape of the in-situ data respect the other AC models. Our findings are consistent with (Wu et al. 2015; Kaufman and Sendra 1988), which showed that ACOLITE, iCOR and Sen-2COR perform better in meso- and hypereutrophic waters than in oligotrophic waters. However, none of the AC models performed well over the entire bandset (444–865 nm). Although the applied AC modules compared use different methodology ACOLITE and iCOR performed similarly. ACOLITE performed best in the 740 nm band, whereas iCOR had good performance in the band 704 nm. iCOR is the only processor in which the adjacency adjustment comes before the atmospheric correction. Moses et al. (2017) identified several issues regarding iCOR. First, unless there is some pixel land present in the image, the surface reflectance

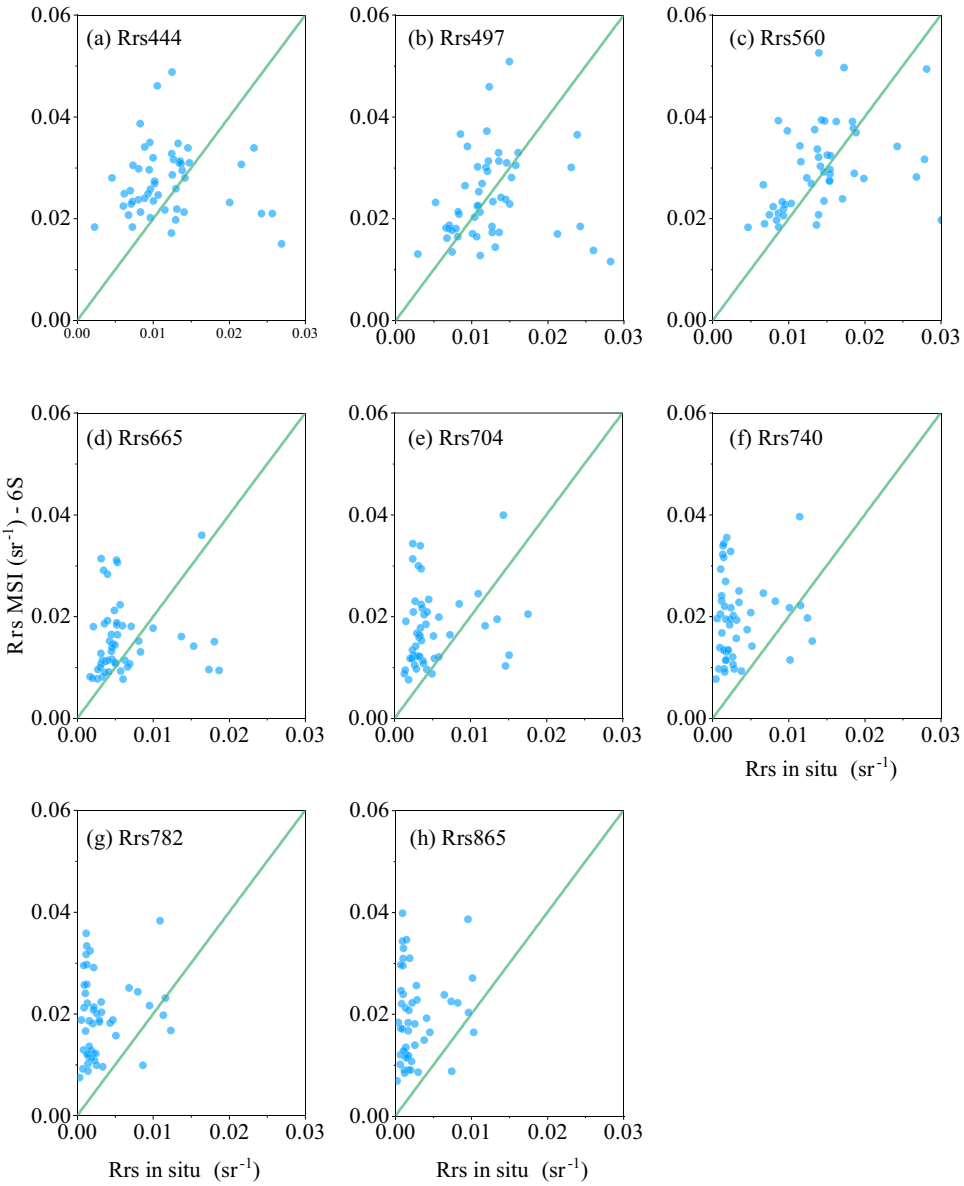


**Fig. 7.** 6SV per-band scatterplot

of the ocean and inlands water cannot be represented by a linear combination of two pure green and one bare soil endmembers. Once this requirement is not achieved, they advised the user to be specific to specify an Atmospheric Optical Thickness (AOT) value suitable for each area. This factor could explain bad results with default setting. C2RCC performs better at the wavelength of 832.8 nm. The poor performance of the algorithm may be induced by insufficient atmospheric correction of a strong Rayleigh scattering. Given that the amplitude of water-leaving reflectance appears to scale with the shapes of the C2RCC RMSD plot in Fig. 9, which suggests that aerosol scattering is not the main factor. We must also consider that waves and currents regularly cause water surfaces to be in motion, scattering the sunlight in various directions, blurring the areas, and causing the radiance received by the sensor to be greater than the radiance emitted by the water surfaces (Matthews 2011).

For the Sen2COR and 6SV AC models, RMSD ranged between 0.0235 and 0.0165, respectively. The low performance of the algorithms can be due to the DDV method, which is better suited for atmospheric correction of land scenes (Bassani et al. 2015). The main reason behind the bad performance of 6SV correction is the complex parameter settings of 6SV. Necessary parameters such as aerosol optical depth (AOD) and water vapor (WV) are crucial to the accurate retrieval of surface reflectances (Zhou et al. 2021). In addition, inaccurate assumptions on aerosol microphysics, which are especially critical to atmospheric accuracy, lead to poor correction results (Kharazmi et al. 2023; Martins et al. 2017). Another critical factor influencing 6SV performance

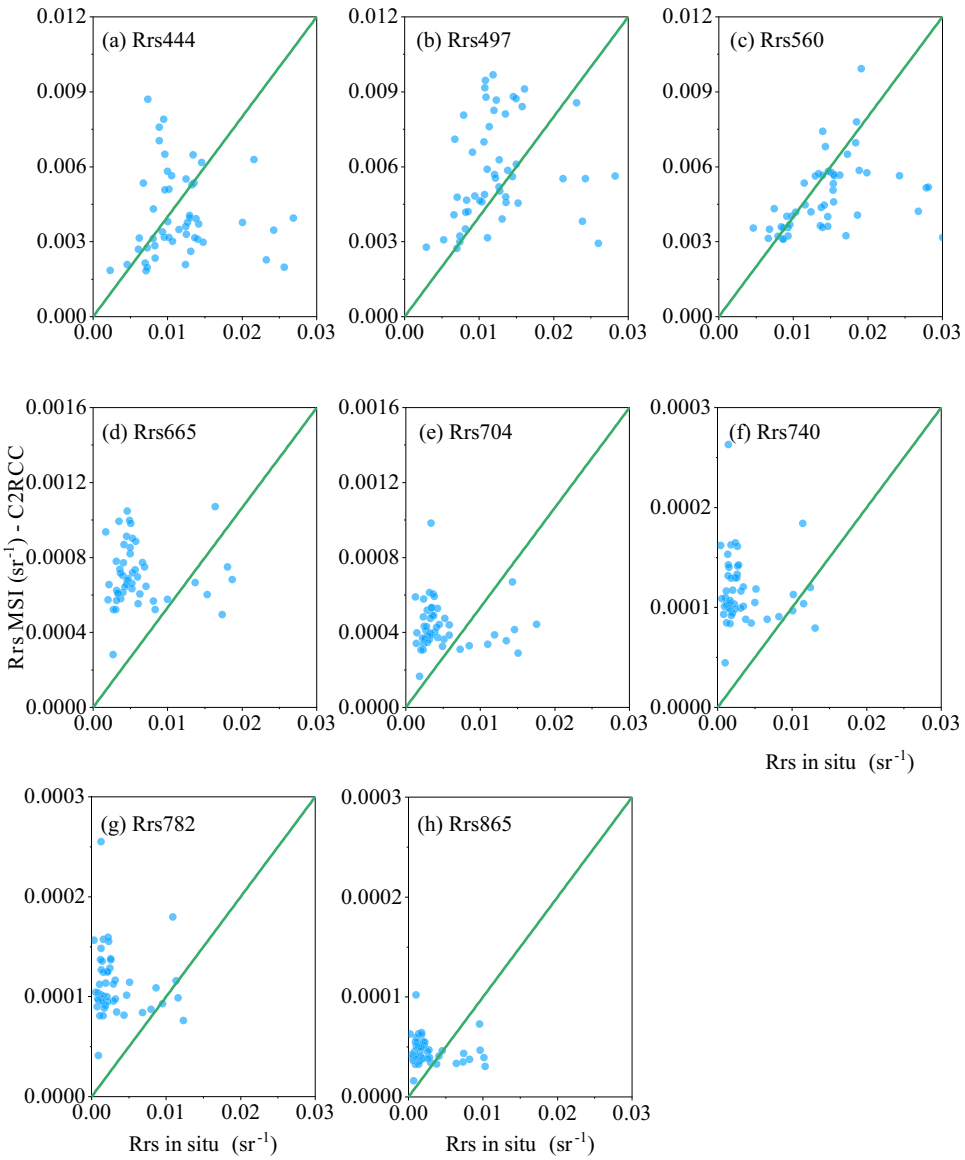


**Fig. 8** C2RCC per-band scatterplot

is the ambient environment of the observation lake. According to Martins et al. (2017), the assumption of homogeneous atmospheric effects over the lake is a large source of error in 6SV result (Shahbandeh and Elhag 2023). The overall performance 6SV algorithm achieves relatively low RMSD and $\psi$ at the wavelengths of 704 nm and 665 nm (Fig. 9), which is consistent with Li et al. (2021b).

We found it necessary to employ a prior classification of water types based on the trophic status of the lakes. The classification is determined by the Chl-*a* values measured directly on-site and is divided into three categories: Type 1, which represents ultra-to-oligotrophic conditions; Type 2, indicating mesotrophic-to-eutrophic conditions; and Type 3, signifying hypertrophic conditions (Harmel et al. 2018). The categorization of water types serves the purpose of helping us comprehend how various atmospheric correction (AC) processors perform. For instance, the AC algorithm may not have been trained for a specific range of inherent optical properties (IOPs), or it may influence the magnitude of the adjacency effect (AE) in the visible bands (Liu et al. 2015). The Hyperspectral data spans the 400–900 nm spectrum through a continuous sequence of narrow bands, enabling the data to be averaged utilizing the spectral response MSI function instrument. The system's automation will guarantee the validation of new sensors and algorithms over significantly shorter timeframes and across a broader range of atmospheric and water conditions than what was previously accomplished.

## 5 Recommendations and Limitations

The high variability of the dataset could help better understand the performance of the different ACs, considering several new variables. The combination of the two

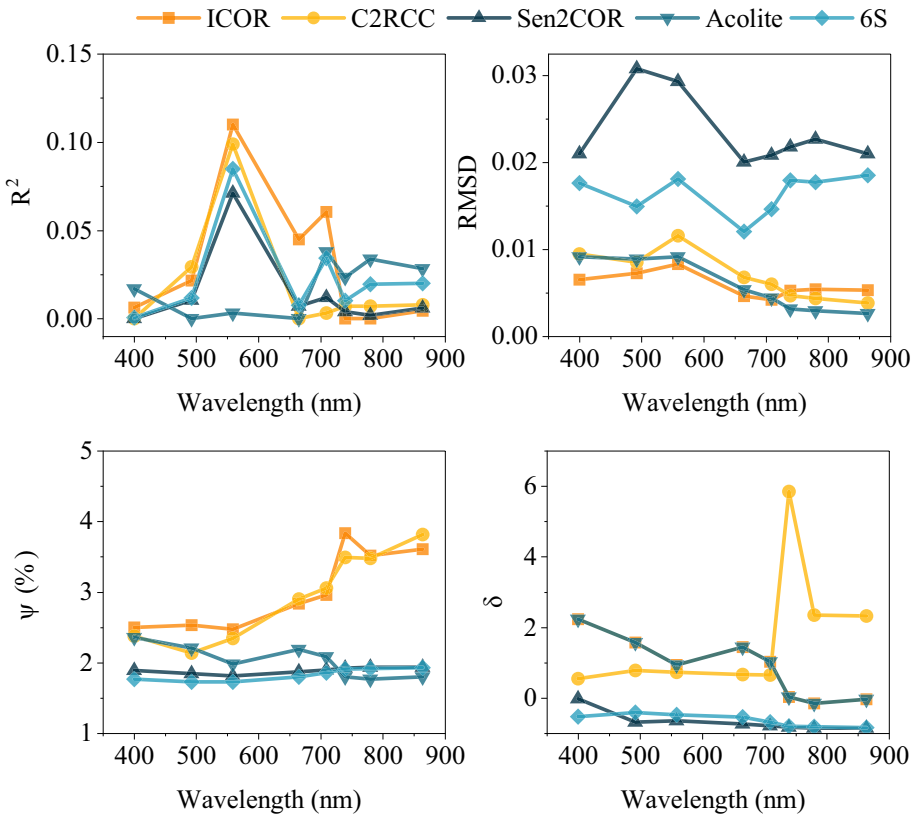


**Fig. 9** S2-MSI wavelength against the used AC algorithms

Sentinel-2 satellite missions will increase the revisit time of measurements over the lake, helping monitor many processes. However, the algorithms are considered mature and are in use, so it is appropriate to test their current performance. However, the size of the dataset is still limited and prevents further analysis of the performance of AC processors, an increase in the number of match-up points leads to more robust statistics, and including more water bodies in the dataset gives further information on the performance under varying atmospheric conditions. With a much larger dataset and associated observations on the optical properties, it will be giving further information and possible targeting of water bodies with specific AC processors. Different available sensors (e.g., Landsat 5, Landsat 7, Advanced Spaceborne Thermal Emission and Reflectance Radiometer (ASTER)) and Synthetic Aperture Radar (SAR) will be applied in values assessment (Naz et al. 2021; Allama et al. 2021).

## 6 Conclusions

Through the analysis of the five atmospheric correction processors to S2-MSI, the main objective of this study was to evaluate the retrieved reflectance acquired from S2-MSI by comparing it with the in-situ reflectance measurements. The statistical linearity reveals that the algorithms with the least errors are ACOLITE and iCOR. The analysis by spectral band helps identify each processor's strengths and weaknesses in the visible and near-infrared spectrum. More match-up points result in more accurate statistics, and increasing the number of water bodies to the dataset would provide more details on how the system performed under various climatic circumstances. Finally, because of the good water reflectance results obtained with ACOLITE and iCOR, it is conceivable to justify the applicability of S2-MSI in estimating inland water quality that will be functional and validated in our next paper. The data fusion of Sentinel-3 and Sentinel-2 sensors will upsurge the temporal resolution of the measurements over lakes, assisting in the monitoring of algal blooms, which are very dynamic and take place in a short time. As the major dam in eastern China, Qiandao Lake has been subjected to anthropogenic disturbance rising with an increasing activity within the lake catchment. It is important to improve the monitoring processes of water environment variability which aids environmental management, and the sustainable ecological conservation plans in this region. EO technique provides a fast and inexpensive monitoring system (Pisanti et al. 2022). In water monitoring studies, atmospheric correction is an important step. In addition, this might be an effective tool for monitoring water quality and providing a framework for making decisions that safeguard public health (Senta et al. 2018).

This study enhances our overall understanding of atmospheric correction techniques for Sentinel-2A imagery over inland waters. By systematically evaluating and comparing different algorithms, the study provides valuable insights into their strengths, weaknesses, and performance in these specific environments. This improved understanding allows researchers, scientists, and remote sensing experts to make more informed decisions when selecting and applying atmospheric correction algorithms for inland water bodies. Moreover, the article highlights the challenges associated with atmospheric correction in such settings, such as water turbidity and adjacency effects, and proposes potential solutions to address these issues. The findings of this research article contribute to the advancement of the field by providing a solid foundation for future studies and the development of improved algorithms for accurate and reliable atmospheric correction over inland waters using Sentinel-2A imagery.

## Appendix 1

See Table 3.

**Table 3** Statistics for the match-ups in the Qiandao Lake

| AC | $\lambda$ | $N$ | $R^2$ | RMSD | $\Psi$ | $\delta$ | Intercept | Slope |
|---|---|---|---|---|---|---|---|---|
| iCOR | B1 | 51 | 0.006 | 0.007 | 314 | 2.2237 | 0.01 | 0.216 |
| | B2 | 51 | 0.022 | 0.007 | 339.1469 | 1.5647 | 0.01 | 0.342 |
| | B3 | 51 | 0.11 | 0.008 | 294.1938 | 0.9312 | 0.008 | 0.795 |
| | B4 | 51 | 0.045 | 0.005 | 680.5864 | 1.436 | 0.004 | 0.528 |
| | B5 | 51 | 0.061 | 0.004 | 906.7716 | 1.0248 | 0.003 | 0.493 |
| | B6 | 51 | 0 | 0.005 | 6833.512 | 0.0254 | 0.003 | 0.002 |
| | B7 | 51 | 0 | 0.005 | 3269.444 | −0.163 | 0.003 | 0.007 |
| | B8 | 51 | 0.005 | 0.005 | 4035.6806 | −0.0422 | 0.003 | 0.039 |
| ACOLITE | B1 | 39 | 0.009 | 2.3556 | 226.7839 | 0.014 | −0.415 | 0.009 |
| | B2 | 39 | 0.009 | 2.2043 | 160.0765 | 0.013 | 0.016 | 0.009 |
| | B3 | 39 | 0.009 | 1.9821 | 95.9519 | 0.013 | 0.21 | 0.009 |
| | B4 | 39 | 0.005 | 2.1864 | 153.5972 | 0.006 | 0.019 | 0.005 |
| | B5 | 39 | 0.004 | 2.0857 | 121.8235 | 0.004 | 0.455 | 0.004 |
| | B6 | 39 | 0.003 | 1.7974 | 62.7227 | 0.003 | 0.255 | 0.003 |
| | B7 | 39 | 0.003 | 1.763 | 57.9401 | 0.002 | 0.276 | 0.003 |
| | B8 | 39 | 0.003 | 1.799 | 62.955 | 0.002 | 0.244 | 0.003 |
| C2RCC | B1 | 51 | 0 | 0.009 | 237.7906 | 0.5458 | 0.012 | −0.022 |
| | B2 | 51 | 0.029 | 0.009 | 136.3033 | 0.7768 | 0.01 | 0.442 |
| | B3 | 51 | 0.099 | 0.012 | 221.2517 | 0.7293 | 0.008 | 1.364 |
| | B4 | 51 | 0 | 0.007 | 794.254 | 0.6549 | 0.006 | −0.406 |
| | B5 | 51 | 0.003 | 0.006 | 1134.8336 | 0.6468 | 0.006 | −1.791 |
| | B6 | 51 | 0.007 | 0.005 | 3093.1622 | 5.8431 | 0.004 | −8.357 |
| | B7 | 51 | 0.007 | 0.004 | 2979.2524 | 2.3445 | 0.004 | −8.233 |
| | B8 | 51 | 0.008 | 0.004 | 6523.4266 | 2.3181 | 0.004 | −18.338 |
| Sen2COR | B1 | 51 | 0 | 0.021 | 237.7906 | 0.5458 | 0 | 0 |
| | B2 | 51 | 0.01 | 0.031 | 136.3033 | 0.7768 | 0.01 | 0.065 |
| | B3 | 51 | 0.071 | 0.029 | 221.2517 | 0.7293 | 0.007 | 0.181 |
| | B4 | 51 | 0.007 | 0.02 | 794.254 | 0.6549 | 0.005 | 0.054 |
| | B5 | 51 | 0.012 | 0.021 | 1134.8336 | 0.6468 | 0.003 | 0.063 |
| | B6 | 51 | 0.004 | 0.022 | 3093.1622 | 5.8431 | 0.004 | −0.026 |
| | B7 | 51 | 0.002 | 0.023 | 2979.2524 | 2.3445 | 0.004 | −0.015 |
| | B8 | 51 | 0.006 | 0.021 | 6523.4266 | 2.3181 | 0.003 | −0.024 |
| 6SV | B1 | 51 | 0.001 | 0.018 | 58.2695 | −0.5373 | 0.012 | −0.018 |
| | B2 | 51 | 0.012 | 0.015 | 53.2945 | −0.4198 | 0.011 | 0.067 |
| | B3 | 51 | 0.085 | 0.018 | 52.8468 | −0.4839 | 0.009 | 0.188 |
| | B4 | 51 | 0.008 | 0.012 | 62.8771 | −0.5479 | 0.005 | 0.053 |
| | B5 | 51 | 0.034 | 0.015 | 71.4537 | −0.6896 | 0.003 | 0.099 |
| | B6 | 51 | 0.01 | 0.018 | 80.3369 | −0.8034 | 0.003 | 0.042 |
| | B7 | 51 | 0.019 | 0.018 | 81.9241 | −0.8192 | 0.002 | 0.057 |
| | B8 | 51 | 0.02 | 0.019 | 84.0668 | −0.8407 | 0.002 | 0.045 |

**Funding** This research was funded by FY-3 Lot 03 Meteorological Satellite Engineering Ground Application System Ecological Monitoring and Assessment Application Project (Phase I): ZQC-R22227, National Natural Science Foundation of China (42201384), and National Natural Science Foundation of China (42171357).

**Data Availability** The data presented in this study are available on request from the corresponding website.

## Declarations

**Conflict of interest** All the authors declare that there is no conflict of interest.

## References

Allama M, Mhawej M, Meng Q, Faour G, Abunnasr Y, Fadel A, Xinli H (2021) Monthly 10-m evapotranspiration rates retrieved by SEBALI with Sentinel-2 and MODIS LST data. Agric Water Manag 243:106432

Bassani C, Manzo C, Braga F, Bresciani M, Giardino C, Alberotanza L (2015) The impact of the microphysical properties of aerosol on the atmospheric correction of hyperspectral data in coastal waters. Atmos Meas Tech 8(3):1593–1604

Berk A, Anderson GP, Acharya PK, Bernstein LS, Muratov L, Lee J, Fox, M, Adler-Golden SM, Chetwynd JH Jr, Hoke ML, et al (2006) MODTRAN5: 2006 update. In: Algorithms and technologies for multispectral, hyperspectral, and ultraspectral imagery XII, pp 508–515

Bresciani M, Cazzaniga I, Austoni M, Sforzi T, Buzzi F, Morabito G, Giardino C (2018) Mapping phytoplankton blooms in deep subalpine lakes from Sentinel-2A and Landsat-8. Hydrobiologia 824(1):197–214

Brockmann C, Doerffer R, Peters M, Kerstin S, Embacher S, Ruescas A (2016) Evolution of the C2RCC neural network for Sentinel 2 and 3 for the retrieval of ocean colour products in normal and extreme optically complex waters. ESASP 740:54

Carlson RE (1977) A trophic state index for lakes 1. Limnol Oceanogr 22:361–369

De Keukelaere L, Sterckx S, Adriaensen S, Knaeps E, Reusen I, Giardino C, Bresciani M, Hunter P, Neil C, Van der Zande D, Vaiciute D (2018) Atmospheric correction of Landsat-8/OLI and Sentinel-2/MSI data using iCOR algorithm: validation for coastal and inland waters. Eur J Remote Sens 51(1):525–542

Dona C, Chang N-B, Caselles V, Sánchez JM, Camacho A, Delegido J, Vannah BW (2015) Integrated satellite data fusion and mining for monitoring lake water quality status of the Albufera de Valencia in Spain. J Environ Manag 151:416–426

Doxani G, Vermote E, Roger JC, Gascon F, Adriaensen S, Frantz D, Hagolle O, Hollstein A, Kirches G, Li F, Louis J, Mangin A, Pahleva N, Pflug B, Vanhellmont Q (2018) Atmospheric correction inter-comparison eXercise. Remote Sens (basel) 10(2):352

Drusch M, Del Bello U, Carlier S, Colin O, Fernandez V, Gascon F, Hoersch B, Isola C, Laberinti P, Martimort P (2012) Sentinel-2: ESA's optical high-resolution mission for GMES operational services. Remote Sens Environ 120:25–36

Gao B-C, Montes MJ, Davis CO, Goetz AFH (2009) Atmospheric correction algorithms for hyperspectral remote sensing data of land and ocean. Remote Sens Environ 113:S17–S24

Gordon HR (1978) Removal of atmospheric effects from satellite imagery of the oceans. Appl Opt 17(10):1631–1636

Gordon HR (1997) Atmospheric correction of ocean color imagery in the earth observing system era. J Geophys Res Atmos 102(D14):17081–17106

Gordon HR, Wang M (1994) Influence of oceanic whitecaps on atmospheric correction of ocean-color sensors. Appl Opt 33(33):7754–7763

Gordon HR, Clark DK, Hovis WA, Austin RW, Yentsch CS (1985) Ocean color measurements. Adv Geophys 27:297–333

Groetsch PMM, Gege P, Simis SGH, Eleveld MA, Peters SWM (2017) Validation of a spectral correction procedure for sun and sky reflections in above-water reflectance measurements. Opt Express 25(16):A742–A761

Gu Q, Zhang Y, Ma L, Li J, Wang K, Zheng K, Zhang X, Sheng L (2016a) Assessment of reservoir water quality using multivariate statistical techniques: a case study of Qiandao Lake, China. Sustainability 8:243

Gu Q, Hu H, Sheng L, Ma L, Li J, Zhang X, An J, Zheng K et al (2016b) Temporal and spatial variations evaluation in water quality of Qiandao lake reservoir, China. Fresen Environ Bull 25:3280–3289

Guanter L, Del Carmen González-Sanpedro M, Moreno J (2007) A method for the atmospheric correction of ENVISAT/MERIS data over land targets. Int J Remote Sens 28:709–728

Harmel T, Chami M, Tormos T, Reynaud N, Danis P-A (2018) Sunglint correction of the multi-spectral instrument (MSI)-SENTINEL-2 imagery over inland and sea waters from SWIR bands. Remote Sens Environ 204:308–321

Kaufman YJ, Sendra C (1988) Algorithm for automatic atmospheric corrections to visible and near-IR satellite imagery. Int J Remote Sens 9:1357–1381

Kharazmi R, Rahdari MR, Rodríguez-Seijo A, Elhag M (2023) Long-term time series analysis of land cover changes in an arid environment using landsat data: (a case study of Hamoun Biosphere Reserve, Iran). Desert 28(1):123–144

Khattab MFO, Merkel BJ (2014) Application of Landsat 5 and Landsat 7 images data for water quality mapping in Mosul Dam Lake, Northern Iraq. Arab J Geosci 7(9):3557–3573

Kotchenova SY, Vermote EF, Matarrese R, Klemm FJ Jr (2006) Validation of a vector version of the 6S radiative transfer code for atmospheric correction of satellite data. Part I: path radiance. Appl Opt 45:6762–6774

Li T, Zhu B, Cao F, Sun H, He X, Liu M, Gong F, Bai Y (2021a) Monitoring changes in the transparency of the largest reservoir in eastern China in the past decade, 2013–2020. Remote Sens 13:2570

Li H, Kuang R, Song Z (2021b) Evaluation of atmospheric correction methods for sentinel-2 image—a case study of Poyang Lake. Spacecr Recov Remote Sens 42(4):108–119

Liu G, Li Y, Lyu H, Wang S, Du C, Huang C (2015) An improved land target-based atmospheric correction method for Lake Taihu. IEEE J Sel Top Appl Earth Obs Remote Sens 9:793–803

Main-Knorn M, Pflug B, Louis J, Debaecker V, Müller-Wilm U, Gascon F (2017) Sen2Cor for sentinel-2. SPIE 3

Martins VS, Barbosa CCF, De Carvalho LAS, Jorge DSF, Lobo FDL, Novo EMLDM (2017) Assessment of atmospheric correction methods for Sentinel-2 MSI images applied to Amazon Floodplain Lakes. Remote Sens 9(4):322. https://doi.org/10.3390/rs9040322

Matthews MW (2011) A current review of empirical procedures of remote sensing in inland and near-coastal transitional waters. Int J Remote Sens 32(21):6855–6899

Mobley CD (1999) Estimation of the remote-sensing reflectance from above-surface measurements. Appl Opt 38:7442–7455

Mograne MA, Jamet C, Loisel H, Vantrepotte V, Mériaux X, Cauvin A (2019) Evaluation of five atmospheric correction algorithms

over french optically-complex waters for the Sentinel-3A OLCI ocean color sensor. Remote Sens 11(6):668
Moses WJ, Sterckx S, Montes MJ, De Keukelaere L, Knaeps E (2017) Chapter 3—Atmospheric correction for inland waters. In: Mishra DR, Ogashawara I, Gitelson AA (eds) Bio-optical modeling and remote sensing of inland waters. Elsevier, Amsterdam, pp 69–100
Naz S, Iqbal MF, Mahmood I, Allam M (2021) Marine oil spill detection using synthetic aperture radar over Indian Ocean. Mar Pollut Bull 162:111921
Pahlevan N, Schott JR, Franz BA, Zibordi G, Markham B, Bailey S, Schaaf CB, Ondrusek M, Greb S, Strait CM (2017a) Landsat 8 remote sensing reflectance (Rrs) products: evaluations, intercomparisons, and enhancements. Remote Sens Environ 190:289–301
Pahlevan N, Sarkar S, Franz BA, Balasubramanian SV, He J (2017b) Sentinel-2 MultiSpectral Instrument (MSI) data processing for aquatic science applications, demonstrations and validations. Remote Sens Environ 201:47–56
Park Y-J, Ruddick K (2005) Model of remote-sensing reflectance including bidirectional effects for case 1 and case 2 waters. Appl Opt 44(7):1236–1249
Pereira-Sandoval M, Ruescas A, Urrego P, Ruiz-Verdú A, Delegido J, Tenjo C, Soria-Perpinyà X, Vicente E, Soria J, Moreno J (2019) Evaluation of atmospheric correction algorithms over Spanish inland waters for sentinel-2 multi spectral imagery data. Remote Sens 11:1469
Pisanti A, Magri S, Ferrando I, Federici B (2022) Sea water turbidity analysis from Sentinel-2 images: atmospheric correction and bands correlation. Int Arch Photogramm Remote Sens Spatial Inf Sci XLVIII-4/W1-2022:371–378
Pyo J, Hong SM, Jang J, Park S, Park J, Noh JH, Cho KH (2022) Drone-borne sensing of major and accessory pigments in algae using deep learning modeling. GISci Remote Sens 59(1):310–332
Reinersman PN, Carder KL (1995) Monte Carlo simulation of the atmospheric point-spread function with an application to correction for the adjacency effect. Appl Opt 34(21):4453–4471
Richter R (1990) A fast atmospheric correction algorithm applied to Landsat TM images. Int J Remote Sens 11(1):159–166
Santer R, Schmechtig C (2000) Adjacency effects on water surfaces: primary scattering approximation and sensitivity study. Appl Opt 39(3):361–375
Sentas A, Psilovikos A, Karamoutsou L, Charizopoulos N (2018) Monitoring, modeling and assessment of water quality and quantity in River Pinios, using ARIMA models. Desalin Water Treat 133:336–347
Shahbandeh M, Elhag M (2023) Microclimate changes and trend analysis of remotely sensed environmental parameters in West Asia semi-arid region. Environ Dev Sustain 1–15
Simis SGH, Olsson J (2013) Unattended processing of shipborne hyperspectral reflectance measurements. Remote Sens Environ 135:202–221
Simis SGH, Peters SWM, Gons HJ (2005) Remote sensing of the cyanobacterial pigment phycocyanin in turbid inland water. Limnol Oceanogr 50:237–245
Steinmetz F, Deschamps P-Y, Ramon D (2011) Atmospheric correction in presence of sun glint: application to MERIS. Opt Express 19(10):9783–9800
Sterckx S, Knaeps S, Kratzer S, Ruddick K (2015) SIMilarity Environment Correction (SIMEC) applied to MERIS data over inland and coastal waters. Remote Sens Environ 157:96–110
Vanhellemont Q (2019) Adaptation of the dark spectrum fitting atmospheric correction for aquatic applications of the Landsat and Sentinel-2 archives. Remote Sens Environ 225:175–192
Vanhellemont Q, Ruddick K (2015) Advantages of high quality SWIR bands for ocean colour processing: Examples from Landsat-8. Remote Sens Environ 161:89–106
Vanhellemont Q, Ruddick K (2018) Atmospheric correction of metre-scale optical satellite data for inland and coastal water applications. Remote Sens Environ 216:586–597
Vermote EF, Tanré D, Deuze JL, Herman M, Morcette J-J (1997) Second simulation of the satellite signal in the solar spectrum, 6S: an overview. IEEE Trans Geosci Electron 35:675–686
Wang M, Bailey SW (2001) Correction of sun glint contamination on the SeaWiFS ocean and atmosphere products. Appl Opt 40(27):4790–4798
Wang X, Gong Z, Pu R (2018) Estimation of chlorophyll a content in inland turbidity waters using WorldView-2 imagery: a case study of the Guanting Reservoir, Beijing, China. Environ Monit Assess 190(10):1–16
Warren MA, Simis SG, Martinez-Vicente V, Poser K, Bresciani M, Alikas K, Spyrakos E, Giardino C, Ansper A (2019) Assessment of atmospheric correction algorithms for the Sentinel-2A MultiSpectral Imager over coastal and inland waters. Remote Sens Environ 225:267–289
Wu Z, Zhang Y, Zhou Y, Liu M, Shi K, Yu Z (2015) Seasonal-spatial distribution and long-term variation of transparency in N'anjiang Reservoir: Implications for reservoir management. Int J Environ Res Public Health 12:9492–9507
Xu J, Lei S, Bi S, Li Y, Lyu H, Xu J, Xu X, Mu M, Miao S, Zeng S (2020) Tracking spatio-temporal dynamics of POC sources in eutrophic lakes by remote sensing. Water Res 168:115162
Yang M, Hu Z, Liu Q, Ren L, Chen L, Li P et al (2013) Evaluation of water quality by two trophic state indices in Lake Qiandaohu during 2007–2011. J Shanghai Ocean Univ 22:240–245
Zeng S, Li Y, Lyu H, Xu J, Dong X, Wang R, Yang Z, Li J (2020) Mapping spatio-temporal dynamics of main water parameters and understanding their relationships with driving factors using GF-1 images in a clear reservoir. Environ Sci Pollut Res 27:33929–33950
Zhou Y, He B, Fu C, Xiao F, Feng Q, Liu H, Zhou X, Yang X, Du Y (2021) An improved Forel-Ule index method for trophic state assessments of inland waters using Landsat 8 and sentinel archives. GISci Remote Sens 58(8):1316–1334

## Authors and Affiliations

**Mona Allam[1,4] · Qingyan Meng[1,2,3] · Mohamed Elhag[5,6,7,8] · Claudia Giardino[9] · Nicola Ghirardi[9] · Yi Su[10] · Mohammed A. M. Al-Hababi[11] · Massimo Menenti[12]**

✉ Qingyan Meng
mengqy@radi.ac.cn

[1] Aerospace Information Research Institute, Chinese Academy of Sciences, Beijing 100094, China

[2] University of Chinese Academy of Sciences, Beijing 100049, China

[3] Key Laboratory of Earth Observation of Hainan Province, Hainan Aerospace Information Research Institute, Sanya 572029, China

[4] Environment and Climate Changes Research Institute, National Water Research Centre, El Qanater El Khairia 13621/5, Egypt

[5] Department of Water Resources, Faculty of Environmental Sciences, King Abdulaziz University, 21589 Jeddah, Saudi Arabia

[6] State Key Laboratory of Remote Sensing, Aerospace Information Institute, Chinese Academy of Science, Beijing 100101, China

[7] Department of Geoinformation in Environmental Management, CI-HEAM/Mediterranean Agronomic Institute of Chania, 73100 Chania, Greece

[8] Department of Applied Geosciences, Faculty of Science, German University of Technology in Oman, Muscat 1816, Oman

[9] CNR-Institute for Electromagnetic Sensing of the Environmental, Via A. Corti 12, 20133 Milan, Italy

[10] Department of Environmental Science and Engineering, Fudan University, Shanghai 200433, China

[11] School of Computer Science and Technology, Data Mining and High-Performance Computing Lab, University of Chinese Academy of Sciences, Beijing 101400, China

[12] Geosciences and Remote Sensing Department, Delft University of Technology, Stevinweg 12628 CN, Delft, The Netherlands